A Procedure for Performing Nonlinear Pushover Analysis for Tsunami Loading to ASCE 7

Marco Baiguera[1], A.M.ASCE, Tiziana Rossetto[2], A.M. ASCE, Ian N. Robertson[3], M.ASCE; and

Crescenzo Petrone[4]

[1] Research Fellow, Dept. of Civil, Environmental and Geomatic Engineering, University College London,

Gower Street, London, WC1E 6BT, United Kingdom (corresponding author). Email: m.baiguera@ucl.ac.uk

[2] Professor, Dept. of Civil, Environmental and Geomatic Engineering, University College London, Gower

Street, London, WC1E 6BT, United Kingdom

[3] Professor, Dept. of Civil and Environmental Engineering, Univ. of Hawaii at Manoa, Honolulu, HI 96822

[4] Senior Earthquake Analyst, Willis Towers Watson, Lime Street, London, EC3M 7DQ, United Kingdom

ABSTRACT

The new ASCE 7-16 Chapter 6 offers a comprehensive and practical methodology for the design of structures for tsunami loads and effects. While it provides prescriptive tsunami loading and design requirements, Chapter 6 also allows for the use of performance-based nonlinear analysis tools. However, the specifics of load application protocol, and system and component evaluation for such a nonlinear approach are not provided. This paper presents a procedure for performing nonlinear static pushover analysis for tsunami loading within the framework of the ASCE 7-16 Standard. Through this approach, the user can both estimate the effective systemic lateral-resisting capacity of a building and the local component demand. This enables the identification of deficiencies in structural elements with respect to the ASCE 7-16 standard acceptance criteria. To demonstrate the procedure, a prototypical reinforced concrete multi-story building exposed to high tsunami hazard in the US Northwest Pacific coast is assessed. This is a building with sufficient height to provide last-resort refuge for people having insufficient time to evacuate outside the inundation zone. The results of the nonlinear static pushover analyses show that the structural system has sufficient lateral strength to resist ASCE 7-16 prescribed tsunami loads, but fails the checks for component-based loading, with the exterior ground story columns observed to fail in flexure and shear. The example demonstrates that use of the tsunami nonlinear static

27 analysis procedure allows the identification of structural deficiencies such that a targeted strengthening

28 of the building can be conducted, (i.e. flexural and shear strengthening of the seaward and inland

29 columns, for the case study building presented), leading to significantly reduced costs.

30 **Keywords:** Tsunami; ASCE 7 Standard; Nonlinear Static Analysis; Push over analysis.

31 **INTRODUCTION**

32 The catastrophic effects of recent tsunami triggered by large subduction earthquakes in the Indian

33 Ocean (2004) and Japan (2011) have highlighted the tsunami threat posed to many coastal communities

34 in the United States and around the world. Community preparedness in tsunami-prone areas of Alaska,

35 Washington, Oregon, California and Hawaii has improved recently through installation of warning

36 systems and increased preparedness for evacuation. However, there are many communities that have

37 limited access to high ground and have insufficient time for complete horizontal evacuation. Under this

38 scenario, taller buildings could potentially offer a safe haven. Critical facilities and multi-story buildings

39 could be designated as vertical evacuation refuges if they have been designed and constructed to

40 withstand tsunami loads.

41 To increase the resilience of coastal communities and mitigate tsunami damage to important

42 structures, tsunami design procedures are now included in US design codes through the introduction of

43 a new Chapter 6, Tsunami Loads and Effects, in ASCE 7-16, *Minimum Design Loads and Associated*

44 *Criteria for Buildings and Other Structures* (ASCE, 2017a). This design standard has been included by

45 reference in the requirements of the 2018 International Building Code (IBC, 2018), and an extensive

46 guide to the provisions with example applications is now available in Robertson (2020). The ASCE 7-

47 16 tsunami design provisions apply to essential (risk category IV) and critical (risk category III)

48 facilities, and designated tsunami vertical evacuation structures located within the mapped Tsunami

49 Design Zone (TDZ). Although not required by ASCE 7-16, local communities are strongly encouraged

50 to require tsunami design for taller risk category II buildings (residential, commercial, etc.) in the TDZ

51 to provide additional options of refuge-of-last-resort for those unable to evacuate to high ground or to

52 a designated vertical evacuation structure. This also improves community resilience by ensuring that

53 important and substantial buildings survive the tsunami and can be re-occupied relatively soon after the

54 event.

55   The Tsunami Design Zone (TDZ) is the area vulnerable to being inundated by the Maximum

56 Considered Tsunami (MCT), defined as having 2% probability of being exceeded in a 50-year period,

57 equivalent to a 2500-year return period. Figure 1 outlines the main steps for the evaluation of buildings

58 in the TDZ. In essence, ASCE 7-16 defines hydrostatic, hydrodynamic and debris impact loads, load

59 combinations, importance factors and acceptance criteria for two main types of structural checks:

60   1. A systemic check – wherein the structural lateral-force-resisting systems (LFRS) are checked

61   for their adequacy in resisting the prescribed tsunami loading.

62   2. A component-based check – wherein the design strength of each individual structural

63   component is checked for adequacy against an enhanced tsunami loading that accounts for local
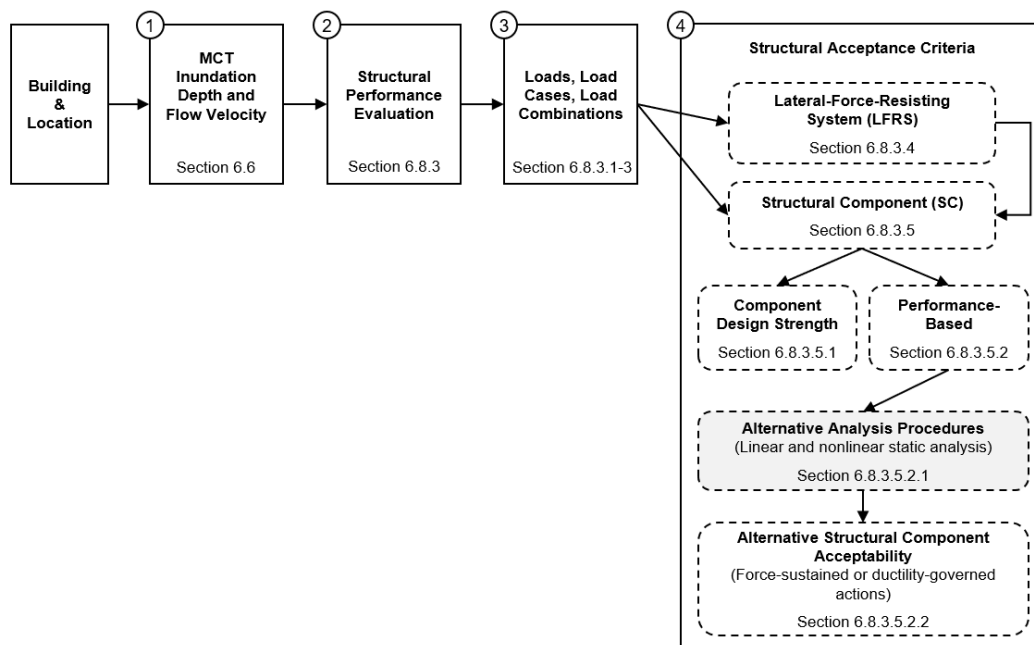
64   drag effects.

Figure 1: Tsunami nonlinear static analysis within the framework of ASCE 7-16 tsunami design provisions (Section numbers refer to ASCE 7-16 (2017a)).

65   Within the ASCE 7-16 standard, a simplified approach is proposed for use in the systemic check.

66 In this simplified check, the acceptance criterion for LFRS is based on a comparison between the

67 tsunami lateral load applied and the structure's seismic design base shear, enhanced to include typical

68 overstrength. For the component-based check, the prescriptive approach is to ensure that the component

69　design strength is larger than the internal forces obtained using a linear elastic, static analysis of the

70　component subjected to the prescribed tsunami loading cases. For structural components that are part

71　of the LFRS, the component internal forces must be combined with internal forces induced by the

72　tsunami loads on the overall building system.

73　　　As an alternative to the simplified systemic check and prescriptive component-based check, the

74　ASCE 7-16 standard allows for the use of performance-based criteria to assess structural response. This

75　includes the adaptation of nonlinear static pushover analysis of ASCE 41-17 (ASCE, 2017b) to tsunami

76　loading. However, no detailed guidance is provided as to how these performance-based methods should

77　be carried out.

78　　　Performance-based engineering methods for tsunami are much less developed than for other

79　hazards, such as earthquakes. For instance, in seismic engineering, nonlinear static and dynamic

80　analysis, generally referred to as pushover analysis and time-history analysis, respectively, are well-

81　established tools for performance-based design and assessment of structures. In reality, pushover

82　analysis is a crude approximation of the highly dynamic loading and induced damage that occurs during

83　a seismic event. However, when applied in the context of tsunami loading, pushover analysis can, in

84　fact, very closely replicate the actual hydrodynamic drag on the overall structure and individual

85　structural components, as these forces are typically of long duration (Foster et al., 2017).

86　　　The complexity of understanding the impact of onshore tsunami inundation on coastal structures,

87　and the challenges in developing inundation models that can simulate realistic tsunami loads and

88　resulting effects, have hampered the development of analytical methods (Rossetto et al., 2018). Recent

89　advances in physical modelling of tsunami and new field observations from tsunami reconnaissance

90　missions have led to the definition of new analysis approaches that apply realistic tsunami loads to the

91　structure and account for the material nonlinearity of structural elements.

92　　　Structural analysis methodologies for tsunami have often been adapted from commonly-used

93　nonlinear static analysis methods for earthquake loading. Macabuag et al. (2014) performed a sensitivity

94　study to compare the structural response of a simple reinforced concrete (RC) frame under different

95　code-based tsunami loadings, including those prescribed by ASCE 7-16. Hydrodynamic forces were

96　applied to each inundated story of the building along the seaward columns, assuming a constant tsunami

4

97   inundation depth and increasing flow velocity. This approach is herein referred to as constant depth

98   pushover (CDPO). CDPO is similar to a seismic pushover analysis, since the lateral tsunami force

99   distribution remains constant while the magnitudes of the individual forces are increased monotonically.

100   Hence, this approach can be implemented easily in structural analysis software that performs seismic

101   pushover analysis. Attary et al. (2017) performed CDPO analyses in a fragility assessment of a low-rise

102   steel moment-resisting frame structure. Random sets of tsunami depth and flow velocity values were

103   used to generate a suite of tsunami forces using the expressions in FEMA P-646 (FEMA, 2012), and

104   were then applied at each story level. Alam et al. (2018) used a similar approach for the fragility

105   assessment of an existing six-story RC school. In the latter, the CDPO analysis approach was

106   implemented applying distributed loading along the vertical structural members and explicitly

107   accounting for the shear failure of columns. The hydrodynamic tsunami force was estimated based on

108   the ASCE 7-16 Standard provisions. Since no specific building location was selected, CDPO analyses

109   were performed using a random suite of inundation depths and velocities.

110   In the context of fragility assessment, Petrone et al. (2017) developed novel approaches for the

111   analysis of structural performance under tsunami loading: namely tsunami time-history dynamic

112   analysis (TDY) and variable depth pushover (VDPO). The TDY procedure follows the same principles

113   as a seismic time-history analysis, apart from the input data, which is the tsunami force estimated from

114   a simulated inundation time-history. In the VDPO analysis, the lateral tsunami force applied to the

115   structure is incrementally increased by monotonically increasing the tsunami inundation depth at the

116   site of the structure. At each depth value, the corresponding flow velocity is calculated assuming a

117   constant Froude number (Fr). A curve of tsunami base shear versus total drift can be plotted from the

118   analysis, and the structural performance is assessed from this tsunami pushover curve at the location

119   where the tsunami base shear equals the applied tsunami loading. TDY and VDPO are shown to provide

120   consistent results in Petrone et al. (2017), Rossetto et al. (2019) and Petrone et al. (2020), with the

121   VDPO analysis outperforming the CDPO analysis in terms of engineering demand parameter

122   estimation, (i.e. inter-story drifts and column shear forces). All these studies have shown that the

123   tsunami fragility of RC buildings is significantly influenced by the occurrence of shear failure in the

124   columns. To capture this effect, the tsunami hydrodynamic loads are discretized into point loads

125 distributed along each column. In addition, the tsunami hydrodynamic force was estimated from

126 experimentally-validated equations by Qi et al. (2014), which account for the regime conditions of the

127 flow impacting the structure and the density of the urban environment.

128   The main limitation of the VDPO as originally conceived is that being a load-control analysis,

129 VDPO is not capable of capturing the degrading portion of the pushover curve. This limitation was

130 overcome by Baiguera et al. (2019) through the development of the VDPO2 approach, which consists

131 of a two-phase nonlinear static analysis. In Phase 1 of the VDPO2, a load-control pushover analysis is

132 conducted assuming that the inundation depth and flow velocity increase incrementally. This phase is

133 essentially a replication of the VDPO. In Phase 2, the analysis switches to response-control pushover

134 analysis, where the displacement is increased incrementally and the corresponding tsunami force is

135 calculated. For the latter force calculation, the same inundation depth and load distribution as in the last

136 step of Phase 1 of the analysis is assumed, with force increase attributed to an increase in the flow

137 velocity (as in the CDPO). The switch from Phase 1 to 2 occurs either when a predefined load level is

138 reached or when the analysis encounters a numerical convergence issue, whichever occurs first. In the

139 latter case, the Phase 1 analysis is repeated up to the time step preceding the numerical convergence

140 issue, and then Phase 2 is initiated.

141   The objective of this paper is to present a methodology whereby the VDPO2 can be applied for

142 tsunami design of buildings located in the TDZ, following the ASCE 7-16 provisions. For ease of

143 reference, this new approach will be termed ASCE-VDPO2. To demonstrate the ASCE-VDPO2

144 approach, a prototypical RC frame selected from the design examples in Robertson (2020) is used as a

145 case study. The advantages of using a pushover analysis approach for design compared to the

146 prescriptive acceptance criteria of the ASCE 7-16 provisions are discussed.

147 **TSUNAMI LOADING**

148   The ASCE 7-16 Chapter 6, Tsunami Loads and Effects, provides a practical methodology to

149 calculate the overall and component tsunami loads on a structure. These are presented in this section as

150 they are adopted in the proposed ASCE-VDPO2 analysis method for consistency with the standard.

Tsunami Load Calculation for the LFRS Systemic Check

151

152   The tsunami load on a structure, F_T, which is used for conducting the systemic check on the LFRS,

153   is estimated using the following hydrodynamic drag equation:

$$F_T = \frac{1}{2}\rho_s I_{tsu} C_d C_{cx} B(hu^2) \tag{1}$$

154   where ρ_S is the minimum fluid mass density, I_{tsu} is the tsunami importance factor for hydrodynamic

155   loads ($I_{tsu} = 1$ for TRC II buildings,), C_d is the drag coefficient, B is the building width perpendicular

156   to the flow, h is the inundation depth, u is the flow velocity, and C_{cx} is the proportion of closure

157   coefficient (with a minimum value of 0.7, adopted in this study). The drag coefficient C_d varies based

158   on the B/h ratio. Figure 2 plots the tabular C_d-B/h data for rectilinear buildings given in Table 6.10-1

159   (ASCE 2017a), along with the linear interpolations between intermediate values that have been derived

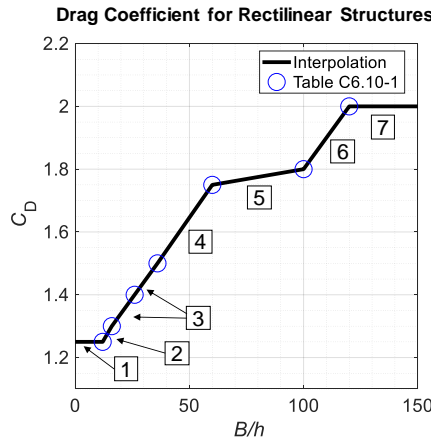160   in this paper. The corresponding equations are provided in the Appendix.

Figure 2: Linear interpolations of drag coefficient-width to inundation depth ratio B/h values from Table C6.10-1
(ASCE, 2017a). Numbers in boxes indicate the curve branches whose equations are provided in Table 1 in the Appendix.

161   For wide buildings, the overall drag is large for small inundation depths due to the large pressure

162   differential between the front and the back, since it takes longer for the water to equalize on opposite

163   sides of the building. The minimum fluid mass density ρ_S is 1127.5 kg/m3, estimated as follows:

$$\rho_s = k_S \rho_{sw} \tag{2}$$

164   where ρ_{sw} is the seawater mass density taken as 1,025 kg/m^3 and k_S is the fluid density factor that

165   accounts for a 10% increase in density due to suspended solids and other small objects, i.e. $k_S = 1.1$.

166   The tsunami depth h and flow velocity u at the structure are assumed by ASCE 7-16 to vary

167   according to the normalized time-history curves in Figure 6.8-1, reproduced here as Figure 3. The

168   curves are normalized to the maximum values of inundation depth, $h_{\max}$, and velocity, $u_{\max}$, at the

169   building site to make them generally applicable. The values of $h_{\max}$ and $u_{\max}$ at a building site can be

170   determined by applying the Energy Grade Line Analysis (Kriebel et al., 2017). No equations are

171   provided by ASCE 7-16 that describe the shape of the normalized time-history curves. Hence, in this

172   paper, to aid with the ASCE-VDPO2 analysis, a least squares error analysis was performed to develop

173   the best fit expressions shown in Table 2 in the Appendix. The maximum lateral hydrodynamic force

174   on the structure, $F_{\mathrm{T,LC2}}$, occurs when the velocity reaches its peak in each direction and the inundation

175   depth is 2/3 of $h_{\max}$. This stage, indicated as Load Case 2 (LC2), controls the design of the LFRS.
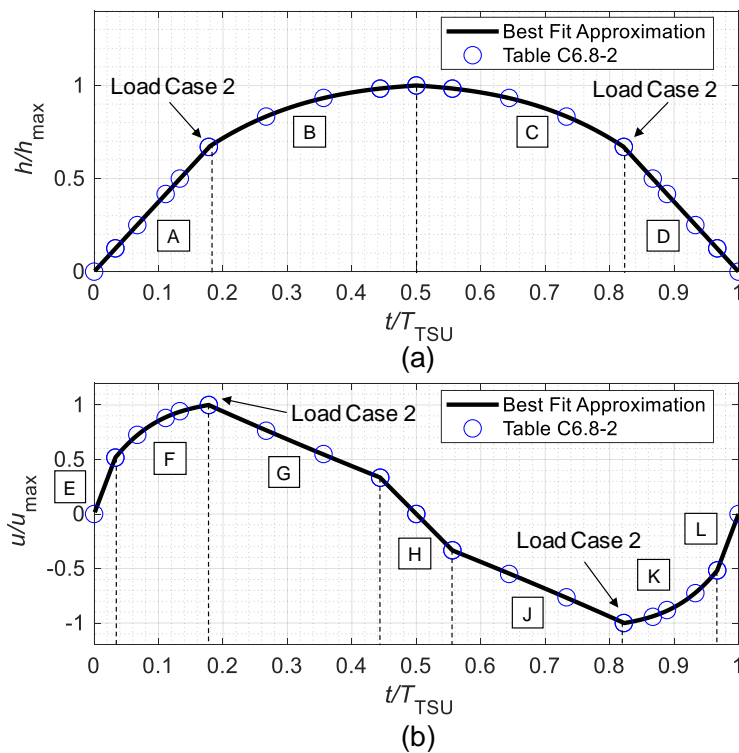

Figure 3: Best-fit approximations of the normalized time inundation depth (a) and flow velocity (b) curves from Figure 6.8-1 and Table C6.8.2 (ASCE, 2017a). Letters in square boxes indicate the branches of the curves. The corresponding best-fit equations are provided in Table 2 in the Appendix.

176   Figure 4 shows typical tsunami time-history curves together with the resulting lateral hydrodynamic

177   force on the overall building from Eqn. (1). The curves are derived for the case-study building presented

178   later in this paper, which is sited in Seaside, Oregon, and is 77.4 m wide in the direction perpendicular

179   to the tsunami flow. At the building site, $h_{\max}$ and $u_{\max}$, are 9.57 m and 11.56 m/s, respectively.
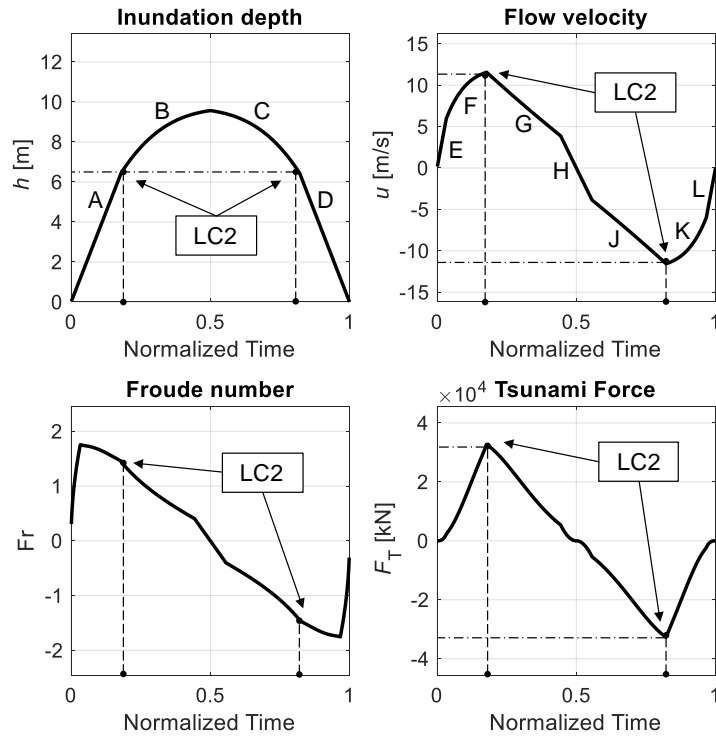
Figure 4: Example of tsunami inundation time-history curves for the case-study building in Seaside, Oregon.

180   ASCE 7-16 requires that tsunami loads be combined with other loads according to the load

181   combinations provided in ASCE 7-16 Section 6.8.3.3 as:

$$0.9D + F_{\text{TSU}} + H_{\text{TSU}} \tag{3}$$

$$1.2D + F_{\text{TSU}} + 0.5L + 0.2S + H_{\text{TSU}} \tag{4}$$

182   where D is the dead load, L is the live load, S is the snow load, F_{tsu} is the tsunami load for incoming

183   and receding directions of flow, and H_{TSU} is the load caused by tsunami-induced lateral foundation

184   pressures developed under submerged conditions. The load combinations given in Eqns. (3) and (4) are

185   consistent with the Extraordinary Load Combinations specified in ASCE 7-16 Section 2.5.

186   **Tsunami Load Calculation for the Component-based Check**

187   All structural components that are part of the LFRS are subjected to the net resultant of their

188   participation in resisting the overall drag force (Eqn. 1) and the hydrodynamic drag caused by local

189   flow around the individual component. The latter is given by Eqn. (5) and is applied as a distributed

190   load on the projected inundated height h_{e}:

$$F_{\text{d}} = \frac{1}{2} \rho_S I_{\text{tsu}} C_{\text{d}} b (h_{\text{e}} u^2) \tag{5}$$

9

191   where b is the effective width of the component and C_d depends on the shape of the individual member

192   being considered. For all exterior components that are likely to be subjected to debris accumulation, C_d

193    $= 2$ and b is taken as the tributary width multiplied by C_{cx} (ASCE, 2017a).

THE ASCE-VDPO2 NONLINEAR PUSHOVER ANALYSIS FOR TSUNAMI LOADING

195   The VDPO2 structural analysis method presented in Baiguera et al. (2019a, 2019b) is here modified

196   to be consistent with the requirements of ASCE 7-16 and ASCE 41-17. The ASCE-VDPO2 adopts a

197   two-phase analysis approach, with a load-control first phase followed by a response-controlled second

198   phase, as described previously.

Analysis Procedure for Design – ASCE-VDPO2 Phase 1

200   For the systemic check in ASCE 7-16 the strength of the LRFS is checked against the 2,500-year

201   Maximum Considered Tsunami (MCT). In ASCE-VDPO2, therefore, the Phase 1 loading is based on

202   the ASCE 7-16 inundation time histories, presented previously, up to LC2. The tsunami inundation

203   depth is increased monotonically following sector A in Figure 3a, with the corresponding flow velocity

204   given in sectors E and F in Figure 3b at the same time step. Figure 5a illustrates the plots of inundation

205   depth, flow velocity, Froude number and tsunami force time-histories up to LC2 for the case-study
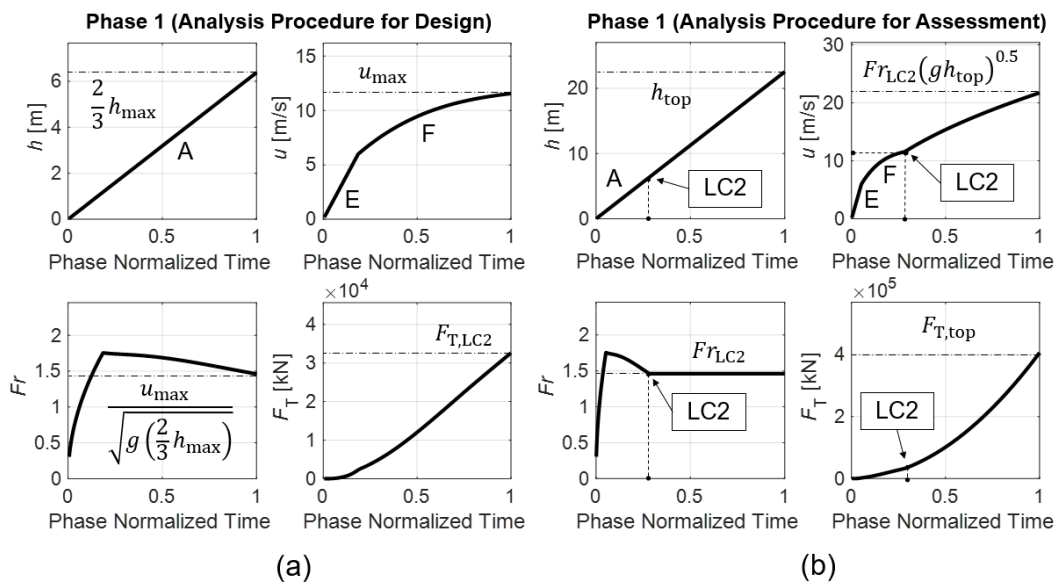
206   building presented later in the paper.

Figure 5: Example of Phase 1 for the case-study building: (a) design; (b) assessment.

Analysis Procedure for Design – ASCE-VDPO2 Phase 2

In Phase 2, the analysis switches to response-control pushover analysis, where the displacement is increased incrementally and the corresponding tsunami force is calculated. The switch from Phase 1 to 2 occurs either when LC2 is reached or when the analysis encounters a numerical convergence issue, whichever occurs first. In the former case, the switch to response-control occurs immediately, with the same inundation depth and load distribution as in LC2 being assumed. In this case, the force increases as the flow velocity increases for the constant inundation depth, $2/3h_{max}$. In the case where numerical instability precedes LC2, the Phase 1 analysis is repeated up to the time step preceding the numerical convergence issue, and then Phase 2 is initiated. The occurrence of a numerical instability before achievement of LC2 does not necessarily mean that the structure has failed before reaching LC2, and the response-control analysis allows the identification of the structural peak capacity, which may or may not exceed the load associated with LC2. For instance, numerical convergence issues might occur during the load-control (Phase 1) due to the inability to capture the degrading branch of the pushover curve.

Analysis Procedure for Assessment – ASCE-VDPO2 Phases 1 and 2

The proposed analysis procedure can also be employed to assess the LFRS for inundation depths and flow velocities larger than the ones for the design basis event (i.e. LC2). Such assessment is performed by first conducting the same Phase 1 analysis as for design up to LC2, and once LC2 is reached, the inundation depth continues to be increased linearly up to the top of the building, with the flow velocity calculated assuming a constant Froude number, taken as the Froude number at LC2, as illustrated in Figure 5b. Similar to before, the switch from Phase 1 to 2 occurs either when the inundation depth equals the building height, or when the analysis encounters a numerical convergence issue, whichever occurs first. In the former case, the switch to response-control occurs immediately, with a constant inundation depth (the building height) used and the same load distribution as in the last step of the Phase 1 analysis. In the case where numerical instability occurs, the Phase 1 analysis is repeated up to the time step preceding the numerical convergence issue, and then Phase 2 is initiated. In this case, Phase 2 assumes a constant inundation depth and the same load distribution as in the last step of the Phase 1 analysis.

235 **LOADING DISCRETIZATION METHODS**

236   The simplified systemic check in ASCE 7-16 compares the overall tsunami force to the design

237 seismic base shear, and does not require a structural analysis per se. However, the component-based

238 check does require an elastic analysis. For conducting the ASCE-VDPO2 analysis a load discretization

239 approach is needed for both systemic and component-based checks. The flowchart in Figure 6

240 summarizes the main steps of the analysis procedure for design.
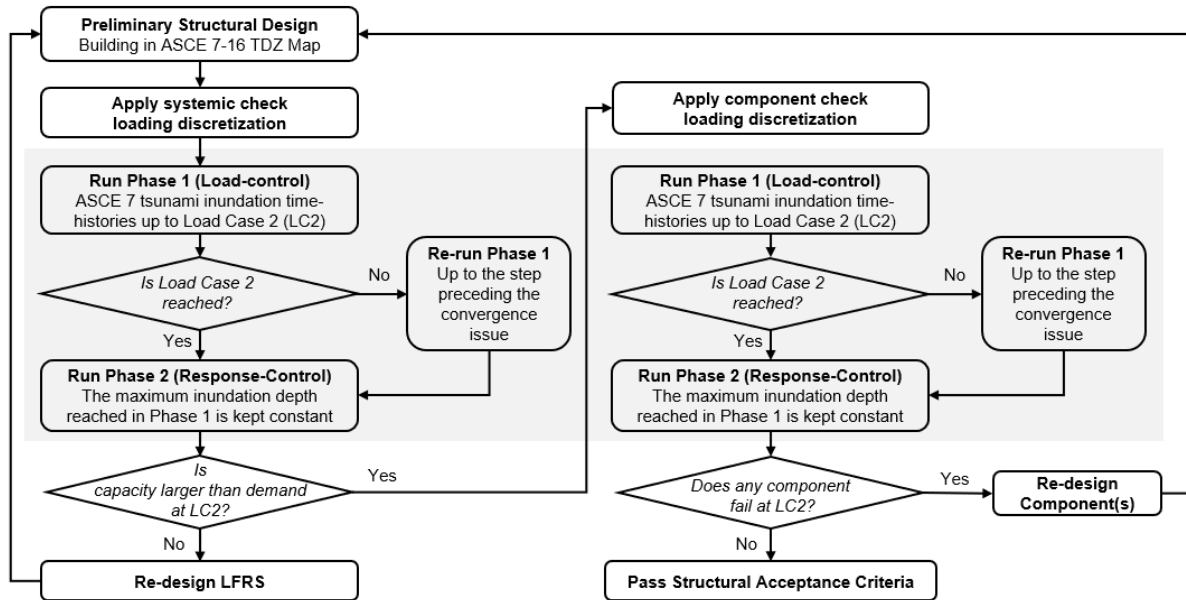
241

242   Figure 6: Flowchart of ASCE-VDPO2 for design.

243 **Systemic Check Load Discretization**

244   ASCE 7-16 specifies that the systemic tsunami lateral load on the building be considered as

245 uniformly distributed on the coastal and inland elevations of the building. The overall tsunami force F_T

246 can be discretized into j forces ($f_{c,j}$), each applied to a line of external columns based on their tributary

247 width. Figure 7 illustrates the discretization of F_T for the case-study building presented later.
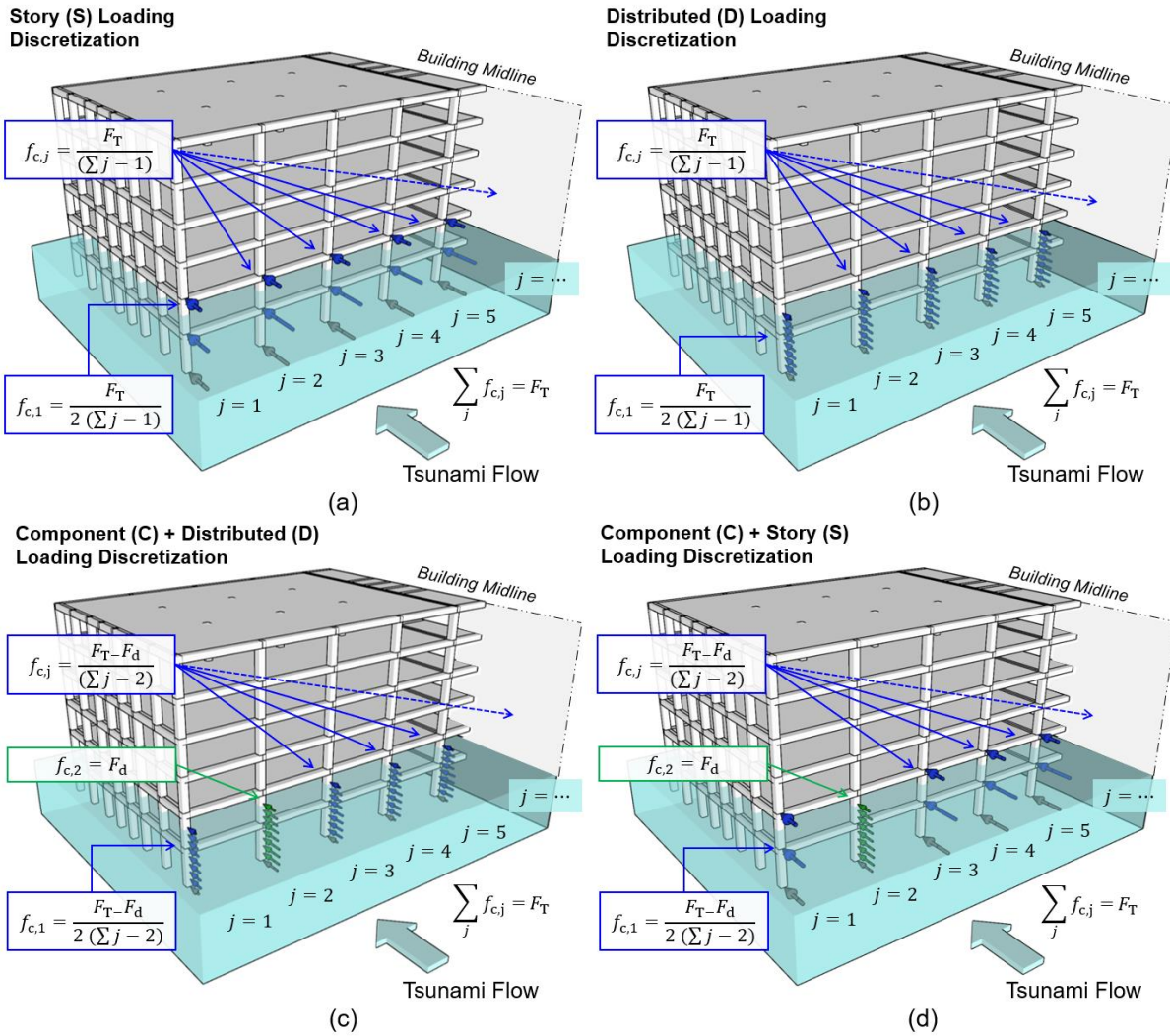
Figure 7: Example of loading discretization methods applied to one half of the case-study building at Load Case 2: (a) *S discretization* for overall hydrodynamic loads (shown in blue color); (b) *D discretization* for overall hydrodynamic loads (shown in blue color); (c) *C+D discretization* for component hydrodynamic loads (with component loads in green color) ; (d) *C+S discretization* for component hydrodynamic loads (with component loads in green color). The loads that are transferred directly to the foundations are shown in grey color to indicate that they are not accounted for in the analyses.

248   However, ASCE 7-16 does not prescribe how the force should be discretized and applied along the

249   columns. An approach used in past studies is to apply nodal loads to each story, referred to hereafter as

250   the *story (S) loading discretization*. The tsunami forces are calculated using a simple influence area

251   approach. As shown in the example in Figure 8a, portion of the load is transferred directly to the

252   foundations (f_1) while portion is applied to the second and third floors (f_2 and f_3). Hence, $f_{c,j,net} =$

253    $f_{c,j}$ - f_1 is the net load resisted by the *j-th* line of exterior columns. If this loading discretization is

254   applied to all exterior columns, as illustrated in Figure 7a, the LFRS will effectively resist only a portion

255   of the overall applied building tsunami load, i.e. $F_{T,net} = \sum_j f_{c,j,net} < F_T$. Hence for *S loading*

256   *discretization*, the net overall tsunami load could be considerably smaller than F_T for buildings with a
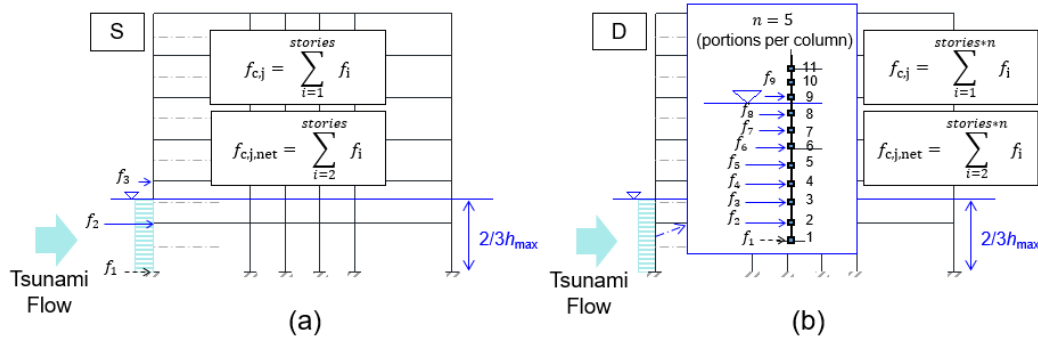
257   tall first floor.

Figure 8: Loading discretization methods: (a) nodal forces applied to stories (*S discretization*); and (b) evenly spaced forces applied to columns (*D discretization*). The loads that are transferred directly to the foundations are dashed to indicate that they are not accounted for in the analyses.

258   An alternative approach is to discretize the same hydrodynamic forces into point loads distributed

259   along each column. This method, referred to hereafter as the *distributed (D) loading discretization*, has

260   been recommended in recent studies (Petrone et al. 2017; Alam et al. 2018), which have shown it to

261   provide the best estimation of demand parameters. If a distributed loading discretization is adopted

262   when using ASCE-VDPO2, it is recommended that for each column, the tsunami loads are applied at 5

263   load application points along the column height, as illustrated in Figures 7b and 8b. In this case, only

264   the load acting on the lower half of the bottom 1/5th of each column is assigned to the column base.

265   The portion of the load transferred directly to the foundations is much smaller than the one calculated

266   in the *S loading discretization*. Hence, $F_{T,net}$ in the *D loading discretization* is comparable in magnitude

267   with F_T.

268   Due to the differences in $F_{T,net}$ arising from the load discretization, it is clear that the *D loading*

269   *discretization* will result in higher shear loads being applied to the LFRS than the *S loading*

270   *discretization*. The *S loading discretization* will instead impart larger moments in the ground story

271   columns due to the loads being applied at a higher level in the structure. In this paper the structural

272   systemic response will be compared for both load discretization assumptions.

273   **Component-Based Check Load Discretization**

274   The ASCE 7-16 design methodology (Figure 1) requires that every structural element be evaluated

275   for component loads. If the structural component is also part of the LFRS, then the internal forces

276 resulting from the component loads must be combined with those resulting from the lateral load on the

277 overall building. Hence, a bespoke loading distribution is proposed in this study, referred to hereafter

278 as the *component (C) loading discretization*.

279   In order to evaluate the combined effect of systemic and component loads on an exterior column

280 that is part of the LFRS, the component drag force given by Eqn. (5) (i.e., F_d with $C_D = 2$) is applied to

281 that column as distributed nodal loads. Simultaneously, the remainder of the building lateral load given

282 by Eqn. (1) (i.e., F_T - F_d) is applied to the remaining columns on the front of the building as distributed

283 loads (Figure 7c) or as nodal loads at each story (Figure 7d). These two options are referred to hereafter

284 as the *C+D* and *C+S loading discretization*, respectively.

285 **CASE-STUDY BUILDING**

286   To demonstrate the ASCE-VDPO2 approach, a case study example is used. This section describes

287 the case study building and the finite element modelling approach used.

288 **Prototype building**

289   A six-story office building is considered as a case-study (Figure 9). The building is located in

290 Seaside, Oregon, which is adjacent to the Cascadia subduction zone and thus characterized by high

291 seismic and tsunami hazards. The Pacific Northwest is at high risk of a potentially destructive tsunami

292 following a Mw 9 earthquake generated along the Cascadia subduction zone (Atwater et al., 1991).

293 Figure 10 illustrates the building location within the ASCE 7-16 2,500-year probabilistic tsunami design

294 zone map of Seaside. Based on the EGLA conducted in McKamey & Robertson (2019), h_{max} and u_{max}

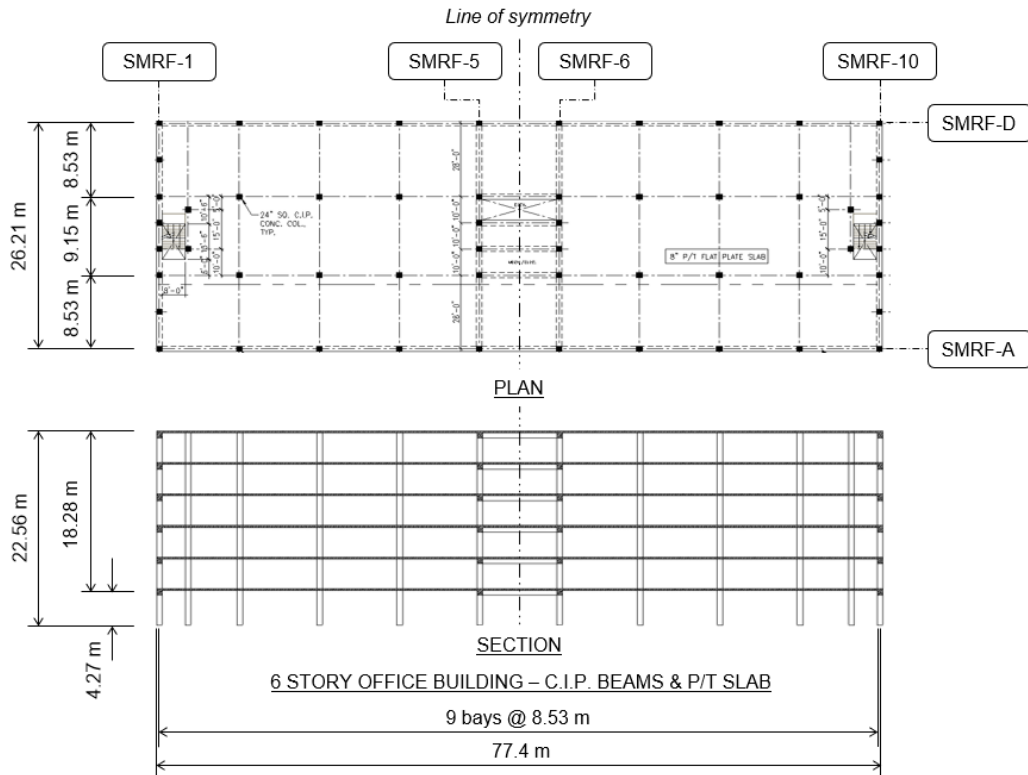295 at the building site are 9.57 m and 11.56 m/s, respectively.

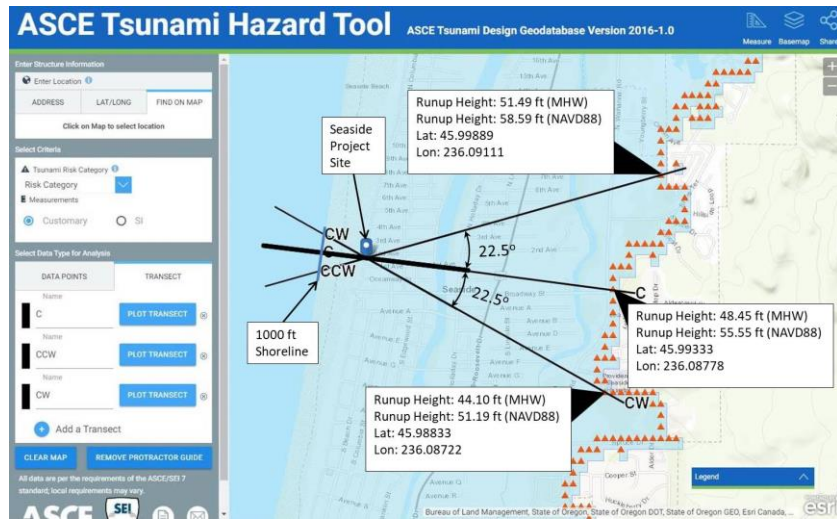Figure 9: Prototype building (McKamey & Robertson, 2019).

Figure 10: Image from the ASCE Tsunami Hazard Tool showing the prototype building location in Seaside, Oregon, along with the three transects used to perform the Energy Grade Line Analysis (from McKamey & Robertson, 2019).

296   The structure is classified as Tsunami Risk Category (TRC) II, and therefore it is not subject to

297   tsunami provisions. However, local jurisdictions are strongly encouraged to require tsunami design for

298   taller TRC II buildings in order to provide secondary refuge-of-last-resort and improve community

299   resilience. Chock et al. (2018) established suitable height thresholds for communities throughout the

300   US Pacific coast, satisfying both the prescriptive acceptance criteria and a recommended height at least

16

301 3.66 m greater than the inundation depth. For the case-study building, the upper three stories would be

302 above $h_{\max}$, hence they could function as a refuge according to the proposal of Chock et al. (2018).

303   The case study building consists of RC special moment resisting frames (SMRF), a flat plate post-

304 tensioned concrete floor system, and interior gravity load columns, as shown in Figure 9. The ground

305 floor consists of a slab-on-grade that is isolated from the building columns. The building was designed

306 for the ASCE 7-16 wind and seismic loads specified for Monterey, California (Robertson, 2020). The

307 building design is appropriate for Seaside, which has similar seismic hazard to Monterey (Seismic

308 Design Category D). Soil classification D for stiff soil is assumed for the building site. The seismic

309 design was carried out assuming the seismic loading combination 1D+0.25L. The corresponding

310 seismic weight is 111,568 kN. The lateral force resisting system consists of four SMRFs in the narrow

311 direction (also the assumed tsunami flow direction), denoted as SMRF-1, 5, 6 and 10, and two moment

312 resisting frames in the wide direction (Figure 9), denoted as SMRF-A and D. According to the design

313 specifications, columns and beams have a nominal compressive strength f_c' of 27.6 MPa and the

314 reinforcing steel has a nominal yield strength f_y of 414 MPa. As illustrated in Figure 11, the size of the

315 columns is uniform along the height of the building, i.e. 71.1x71.1 cm for the SMRFs, and 61x61 cm

316 for the internal gravity load columns, while the size of SMRF beams is 76.2 wide by 61 cm deep. The

317 concrete cover is 5 cm. In the SMRF columns, steel reinforcing ratio varies from 1.3% at the ground

318 floor to 1% at the upper stories. Transverse reinforcement in the SMRF columns consists of seismic

319 hoops with three 12.7-mm-diameter legs at every 10 cm in the column ends (71 cm long) and three 9.5-

320 mm-diameter legs every 15 cm in the central section. More details about the seismic design of the

321 building can be found in Yokoyama and Robertson (2014). Complete tsunami design examples for this

322 building, and a similar shear wall building, located in Seaside, OR, Monterey, CA, Hilo, HI and

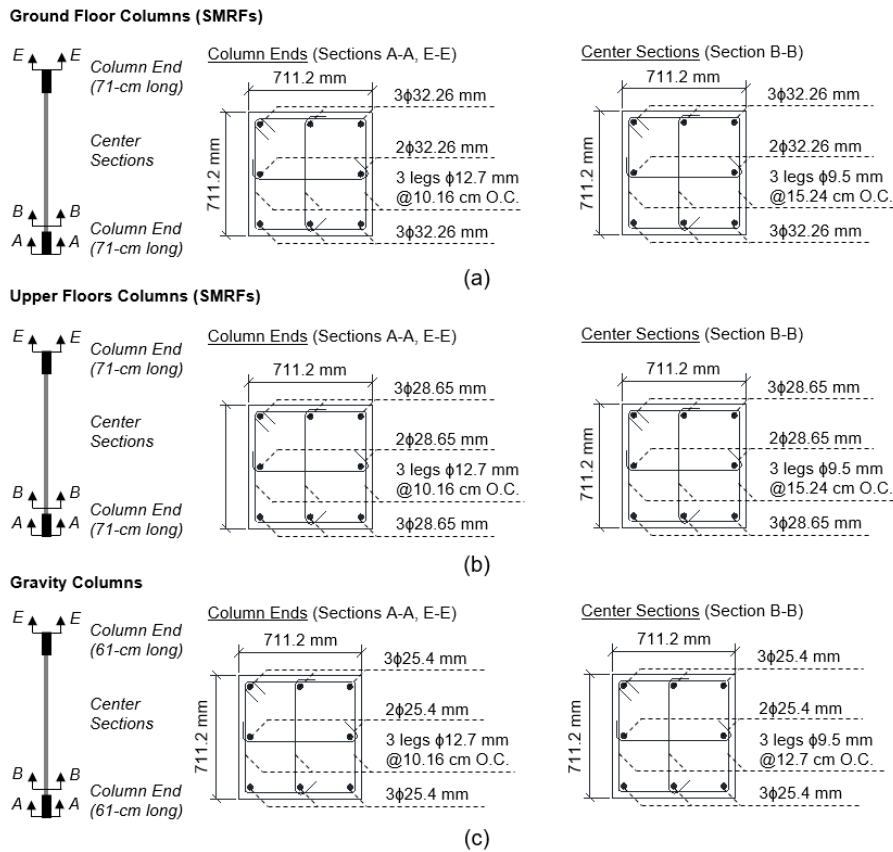323 Waikiki, HI are provided in McKamey and Robertson (2019).

Figure 11: Column cross-section detailing: (a) SMRF columns at ground floor; (b) SMRF columns at upper floors; and (c) gravity columns.

Finite element model

The building is modelled in OpenSees (McKenna et al., 2010) as a two-dimensional model replicating one half of the full structure. Figure 12a illustrates the various components of the model that include: one end moment resisting frame (with 8 columns), one interior moment resisting frame (with 6 columns), six exterior columns that form part of the transverse exterior moment resisting frames (see Figure 12b), and six internal gravity columns. All these components are linked by means of retained-constrained node control so as to simulate the rigid diaphragm at each floor level.
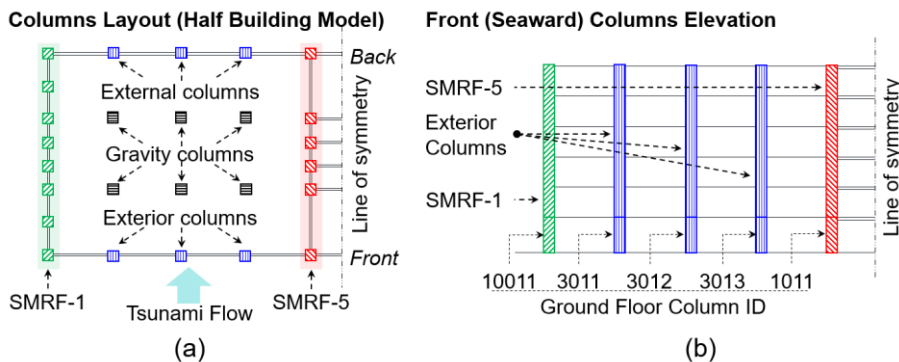

Figure 12: Main structural components for half of case-study building: (a) plan layout; and (b) elevation

331   Beams and columns are modelled using force-based nonlinear beam-column elements. A

332   distributed plasticity model is adopted, since the inelastic behavior due to tsunami pressure can form at

333   any point along the column height. A fiber approach is used for the cross-sections with five integration

334   points along each element.

335   Expected material properties are calculated by multiplying nominal values by appropriate factors

336   in accordance with ASCE 41-17 (ASCE, 2017b). The expected concrete compressive strength is

337   increased by a factor of 1.25, i.e. 41.4 MPa, and 1.50 for reinforcing steel yield and tensile strengths,

338   i.e. 517 MPa and 776 MPa, respectively. Reinforcing steel is assumed to have a strain hardening ratio

339   of 0.0057 and an ultimate steel strain of 0.22. The constitutive material *Concrete04* in OpenSees, based

340   on Uniaxial Popovics material (Popovics, 1973) with an unloading and reloading stiffness model

341   according to Karsan and Jirsa (1969) and exponential decay for the strength, is employed to model

342   confined and unconfined concrete. It is noted that *Concrete04* model simulates stiffness degradation.

343   Concrete within the reinforcement cage is associated with a confined concrete constitutive law (Figure

344   13a), while the cover concrete outside the reinforcement cage is modelled as unconfined (Figure 13b).

345   Due to the low axial forces in the beams, concrete in the beams is modelled as unconfined. The steel

346   stress-strain constitutive material is modelled using the Giuffre-Menegotto-Pinto model (Filippou et al.,

347   1983), named *Steel02* in OpenSees (Figure 13c).

348   Gravity loads are combined with the tsunami loads according to the load combination in Eqn. (3)

349   and are applied to the beams of the transverse frames and to the gravity columns.

350   Validation of the developed numerical model was conducted with respect to an independent model

351   of the same structure in Aegerter, (2021). The latter model is developed in ETABS using a lumped

352   plasticity approach. Comparison of ….. response showed a close agreement (within 5%).

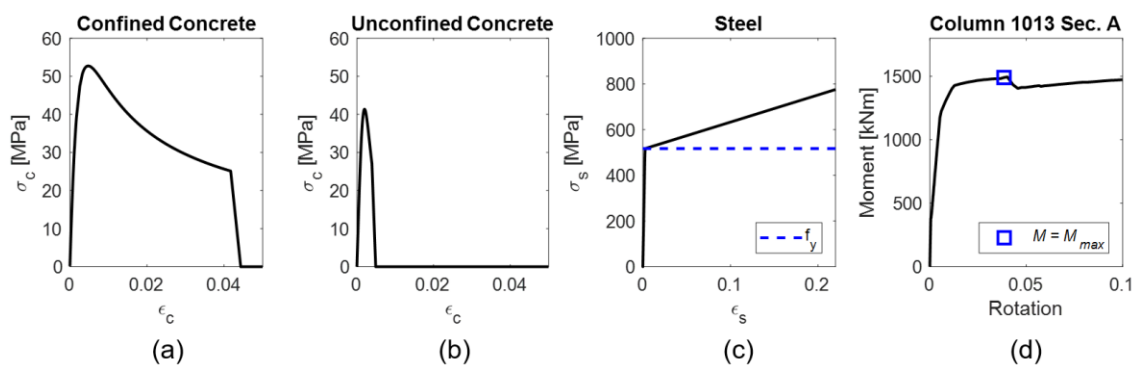
(a)   (b)   (c)   (d)

Figure 13: (a) and (b) *Concrete04* model for confined and unconfined concrete (Mander et al., 1988); (c) *Steel02* model for steel (Filippou et al., 1983); and (d) moment-curvature at the end section of a ground floor column.

Structural Performance Evaluation – Design Systemic Check

353

354   The structural performance is evaluated at an applied tsunami force corresponding to LC2 for the

355   design case. In this check, the maximum strength of the LFRS of the case study building, as calculated

356   using the ASCE-VDPO2 approach, is compared to the LC2 loading. If the tsunami pushover curve

357   shows the building to have a strength larger than the applied loading at LC2, then the systemic check is

358   deemed to have been passed.

359   The performance of individual components of the structure should not be evaluated within the

360   systemic analysis check, as the forces applied to these components are different from those imposed in

361   the component-based check and will not provide the correct target component strengths for design or

362   strengthening. However, as the former component loads are typically lower than in the component-

363   based check, observations of component failures can be indicative of problem areas within the structure.

364   It is noted that, while $C_D = 2$ for component loading, C_D for the corresponding systemic force on the

365   entire building varies from 1.25 to 2.0 and is typically lower than 2 (see Figure 2).

Structural Performance Evaluation – Component-based Check

366

367   In the component-based check, component failure is indicated when either its moment or shear

368   capacity is reached. In particular, previous studies, (Petrone et al., 2017; Alam et al., 2018), have shown

369   that a typical collapse mechanism for RC structures under tsunami loading is the occurrence of shear

370   failure in the columns. This often precipitates global failure if no strengthening measures are adopted.

371   Hence, in this study, shear failure occurrence is tracked in all ground-story columns (i.e. the seaward

372   columns indicated in Figure 12b, which are subjected to the highest shear demand). It is assumed that

373   local shear failure occurs when the shear force at any section of a column exceeds the nominal shear

374   strength calculated according to the formulation of ASCE 41-17 (ASCE, 2017b):

$$V_n = k \left[\alpha \frac{A_v f_y d}{s} + \lambda \left(\frac{0.5\sqrt{f_c'}}{M/Vd} \sqrt{1 + \frac{N}{0.5\sqrt{f_c'} A_g}} \right) 0.8 A_g \right] \quad (6)$$

375   where A_v is the area of shear reinforcement in a single set of hoops, f_y is the shear reinforcement yield

376   strength, d is the effective depth, s is the hoop spacing, $k = 1$ for low ductility demand, $\alpha = 1$ for s/d

377   < 0.75, $\lambda = 1$ for normal-weight aggregate concrete, f_c' is the compressive strength of concrete, A_g is

378   the gross cross-sectional area, N is the axial compressive force (set to zero for tension force), and M/Vd

379   is the aspect ratio, which should not be taken as greater than 4 or less than 2. In this study, it is assumed

380   that $M/V = 0.5 L_{col}$, where L_{col} is the length of the column (e.g. $M/Vd = 3.23$ for ground floor SMRF

381   columns). Since fluid forces on structural components are classified as force-controlled actions in ASCE

382   7-16, the shear strength is calculated using the nominal material properties, in accordance with Figure

383   C10-1 in ASCE 41-17 (ASCE, 2017b). Both the end and center column sections are checked due to

384   differences in their shear reinforcement (Figure 11). The OpenSees model does not evaluate shear

385   failure, so a separate shear check is performed on all columns post-analysis. In addition, to check

386   whether columns experience shear failure before flexural yielding, a further check on the attainment of

387   the maximum flexural moment, i.e. $M = M_{max}$, is performed for the end sections, as illustrated in

388   Figure 13d.

389   **RESULTS**

390   **Prescriptive systemic acceptance criteria**

391   ASCE 7-16 provides a simple criterion to evaluate the systemic tsunami capacity of a seismically-

392   designed structure. This recognizes that a building designed to resist high seismic loading (i.e. Seismic

393   Design Criteria D, E or F), has significantly greater inherent strength than the design seismic base shear,

394   so portion of this overstrength can be utilized to resist the tsunami force (Chock et al., 2018).

395   Effectively, the simplified check implies that the structural lateral force resisting system (LFRS) does

396   not require additional lateral strength when:

$$F_{T,net,LC2} < 0.75 \Omega_0 E_h \tag{7}$$

397   where $F_{T,net,LC2}$ is that portion of the maximum overall building tsunami load, $F_{T,LC2} = 32.603$ kN that

398   is resisted by the LFRS, Ω_0 is the system seismic overstrength factor and E_h is the base shear due to

399   horizontal earthquake forces. As illustrated in Figure 7a, portion of this tsunami load ($f_1 = 10,894$ kN)

400   is transferred directly to the foundations. The remaining $F_{T,net,LC2} = 32,603 - 10,903 = 21,700$ kN must

401   be resisted by the LFRS. For the prototypical building, $\Omega_0 = 3$ (for special MRFs, ASCE 7 Table 12.2-

402   1) and $E_h = 10,831$ kN, hence $\Omega_0 E_h = 32,493$ kN. The applied tsunami force $F_{T,net,LC2} = 21,700$ kN is

403   less than the limit of 0.75·32,493 = 24,370 kN from Eqn. (7). This check indicates that the seismic

404   lateral force resisting system should have sufficient strength to resist the overall tsunami loads.

Systemic check via nonlinear static analysis - design

406   Nonlinear static pushover analyses are employed to evaluate the lateral capacity of the structure to

407   resist tsunami loads. Figure 14a shows the total base shear-top drift curves from the seismic pushover

408   analysis along with the curve from the ASCE-VDPO2 with Phase 1 up to Load Case 2 and *S loading*

409   *discretization*. This load pattern is selected as it is the one currently recommended in the commentary

410   of the ASCE 7-16 for evaluating the lateral force resisting system at LC2 (Robertson, 2020). The

411   tsunami pushover curve shows that the systemic tsunami capacity of the building is significantly larger

412   (by 40%) than the overall net tsunami load at LC2 ($F_{T,net,LC2}/2$= 21,700/2 = 10,850 kN, shown as a

413   thick dashed line in Figure 14). Hence, the structure passes the systemic check of ASCE 7-16 when the

414   tsunami nonlinear pushover analysis is employed. It is noted that the systemic results have been

415   validated by a recent study (Aegerter, 2021), which developed a three-dimensional model of the same

416   building using the commercial software ETABS and employing a more standard lumped-plasticity

417   approach.

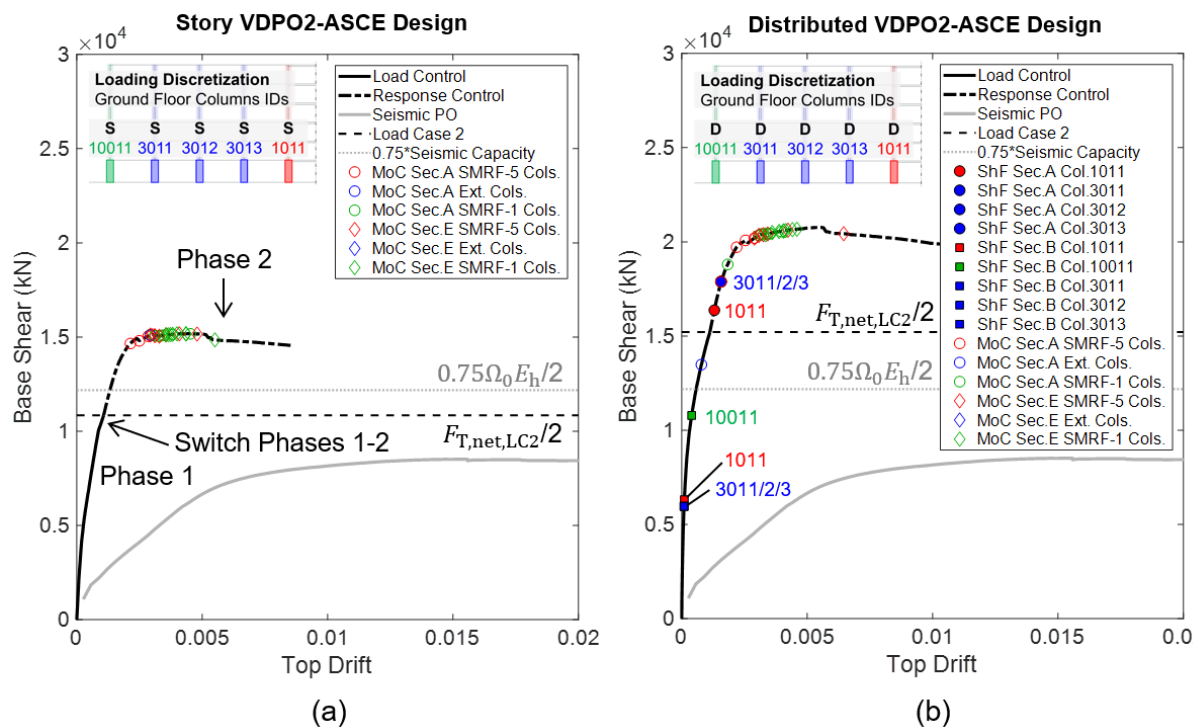(a)   (b)

Figure 14: Base shear-top drift curves of seismic pushover (PO) and ASCE-VDPO2 analyses (Design): (a) *story loading discretization*; and (b) *distributed loading discretization*. Filled and empty markers indicate the attainment of shear failure (ShF) and maximum moment capacity (MoC) in ground floor columns cross-sections (see Figure 11), respectively.

418   A seismic pushover analysis is also performed to draw a consistent comparison between the actual

419   lateral tsunami capacity with the corresponding seismic capacity. The seismic pushover is conducted

420   using a lateral load distribution corresponding to the first mode response (fundamental period = 0.8 s;

421   first mode characterized by 83% mass participation factor). It is observed that under the tsunami lateral

422   loading the case study building exhibits both a significantly increased stiffness and lateral load capacity

423   than under seismic loading. The case study building shows a strength increase under tsunami loading

424   of 1.8 times the seismic response. The difference in response is a natural consequence of the

425   significantly different way in which seismic and tsunami loads act on a building. Tsunami loads are

426   only applied at the lower floors of the building, while the seismic loads are applied at every story of the

427   structure (where the mass is assumed to be concentrated) with increasing magnitude at higher stories.

428   This seismic load distribution therefore results in much larger roof lateral deformations and additional

429   associated P-Delta moments.

430   However, the relationship between the tsunami and seismic strength of a building is not simple to

431   predict. Other studies that have evaluated both the seismic and tsunami base shear capacities of

432   structures using seismic and various tsunami pushover methods (Rossetto et al., 2019; Petrone et al.

433   2020) show tsunami load capacities between 1.5 to 6 times larger than the respective seismic load

434   capacities. These observations cast doubts as to the adequacy of the simplified systemic check within

435   ASCE 7-16, which adopts the seismic design strength of a building as a predictor of its tsunami load

436   resistance. Further questions are raised when the simplified check is conducted here using the actual

437   seismic strength of the case study building instead of that estimated using the assumed overstrength

438   factors. For the case study building, the actual seismic lateral capacity (8,521·2 = 17,042 kN) is larger

439   than the design seismic base shear (E_h = 10,831 kN) as expected but is substantially less than that

440   predicted by the use of an overstrength factor Ω_0 = 3 (32,493 kN). Hence, for this building it is apparent

441   that the overstrength factor assumed in the ASCE 7-16 simplified check significantly overestimates the

442   reserve lateral load capacity. The overstrength factor is used in seismic design to ensure that critical

443   elements remain elastic while the yielding sections develop full plastic hinges. It is therefore biased to

444   being high in order to provide conservative seismic design. The 0.75 factor in Eqn. (7) is intended to

445   compensate for this bias, but it appears that this factor may be optimistic. It is important to note that if

446   the simplified systemic check was conducted with the actual seismic base shear capacity of the structure

447   (as predicted by the pushover), the structure would fail the check and a redesign of the LFRS would be

448   required for it to resist the applied tsunami loads.

449   Due to the complexity in relating the seismic and tsunami strengths of structures it is not known if

450   the simple systemic check allowed in ASCE 7-16 (Eqn. 7) is conservative or not. In most practical cases

451   it is considered that the component checks will dominate the tsunami design/redesign of a structure.

452   Nevertheless, it is recommended in this paper that non-linear structural tsunami analysis be used to

453   conduct the systemic design check of ASCE 7-16 instead of the simplified check.

454   **The influence of load discretization assumptions on the systemic check**

455   As previously described, the $F_{T,net}$ applied in the analyses with S and D loading discretization is

456   different due to the portion of loading that is assumed transferred directly to the structure foundations.

457   Also the center of load application is much higher in the structure for the S loading discretization. The

458   difference in size and location of applied loads results in differences in the structural response under

459   the two loading discretization assumptions.

460   In the *S loading discretization* case, an apparent lower strength and stiffness of the structure is

461   observed. It is seen that the higher level at which the loading is applied induces large moments, as well

462   as shear forces, in the ground story columns of the structure. Bending failure of the columns (indicated

463   by empty markers in Figure 14a) occurs without shear failure of columns. Instead, in the case of the *D*

464   *loading discretization* although the structure is subjected to a larger overall net tsunami force at LC2

465   ($F_{T,net,LC2}/2 = 30,422/2 = 15,211$ kN, slightly smaller than $F_{T,LC2}$), this load is only partially

466   redistributed via the building diaphragms, resulting in larger shear forces than in the ground story

467   columns and an overall increased stiffness and strength of the structure (see Figure 15b) as compared

468   to the *S loading discretization* case. From Figure 14b it can be observed that the larger internal shear

469   forces induce failure in the central portions (i.e. Section B) of the seaward columns, and not in the end

24

470 sections where seismic design requirements for ductile response lead to increased transverse

471 reinforcement (i.e. Section A). It is also noted that columns experience shear failure before flexural

472 yielding, attained at the end cross-sections, i.e. $M = M_{max}$ at Sections A and E illustrated in Figure 14b

473 by empty markers.

474 Despite the significantly different structure responses, the evaluation of the systemic tsunami

475 capacity of the building, using both *D* and *S discretization*, indicates that the structure satisfies the

476 ASCE 7-16 requirement for collapse prevention without additional strengthening. It should be noted

477 that this systemic check is not intended to be used in the evaluation of the individual component

478 capacities (column shear or moment capacity) because this systemic loading does not replicate the

479 component loading required by ASCE 7-16 Section 6.10.2.2. Component assessment for the prototype

480 building is presented later in this paper and it will be seen that the ground floor columns fail the

481 component-based check. However, as the component check applies distributed loads to the component

482 assessed, and as $F_{T,net}$ is larger in the *D load discretization* case, applying the systemic load with the

483 latter load discretization can provide an indication of which columns are likely to be critical when the

484 component assessment is performed.

485 **Systemic check via nonlinear static analysis - assessment**

486 The proposed procedure for tsunami nonlinear static analysis can also be used for assessing the

487 capacity of the building for inundation depths and flow velocities higher than those associated with the

488 MCT, as shown in Figure 5b. Figure 15a shows the total base shear-top drift curves from the seismic

489 pushover analysis and from the ASCE-VDPO2 with extended Phase 1 and *S loading discretization*.

490 While the analysis provides the same results up to LC2, it indicates that the building would have a

491 maximum systemic tsunami capacity of 21,201·2 kN. This force is slightly smaller than those obtained

492 in the previous analyses (see Figure 15b), due to the larger bending actions that result from the increased

493 inundation depths. The peak strength of the structure occurs when $h = 7.25$ m and $u = 12.37$ m/s,

494 compared with $h = 6.38$ m and $u = 11.56$ m/s for LC2. While this would correspond to an event with a

495 return period longer than 2,500 years, it provides a measure of the building's reserve capacity for

496 tsunami loading. The difference between the tsunami load associated with LC2 and the peak strength

497 of the structure is 37% in this case, which provides a reasonable estimate of the extra systemic capacity

498 of the structure.

Component-based check via nonlinear static analysis

500 ASCE 7-16 requires that all structural components be evaluated for hydrodynamic loads and that

501 all exterior structural components also be evaluated for debris impact loads. Debris impact loads are

502 extremely short duration impulsive loads and cannot be represented by pushover analysis. Therefore,

503 this study of pushover analysis for tsunami loads only considers the hydrodynamic loads on the
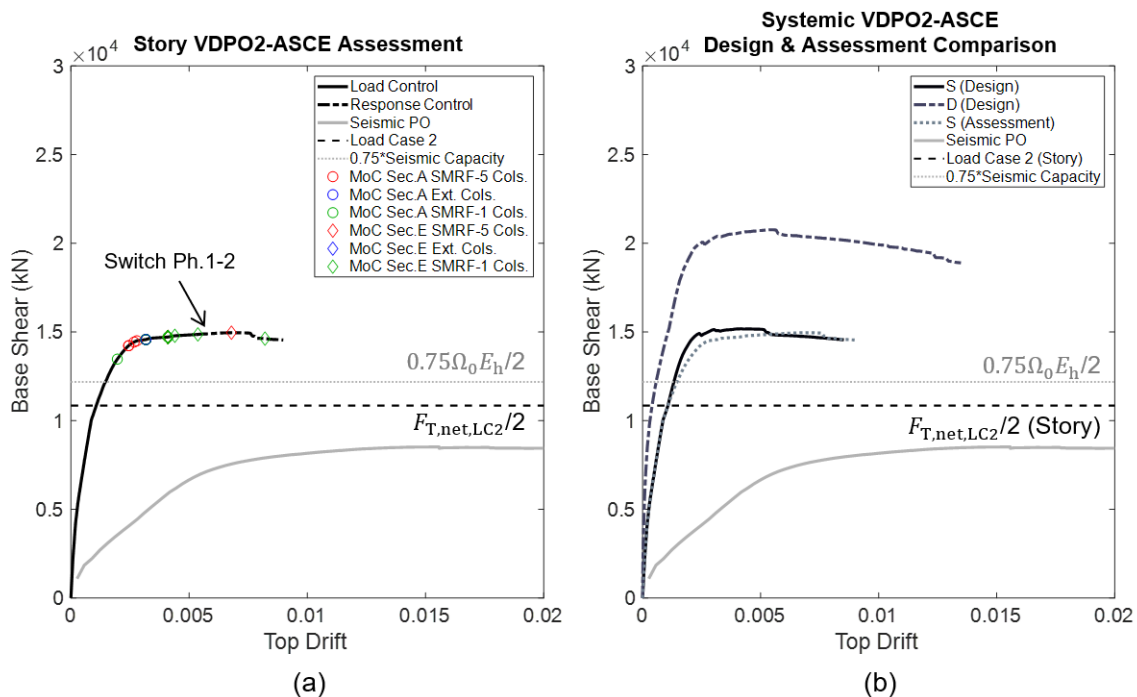
504 structural components.

Figure 15: Base shear-top drift curves from seismic pushover (PO) and ASCE-VDPO2 analyses: (a) ASCE-VDPO2 with Phase 1 for Assessment and *S loading discretization*; and (b) comparison of systemic responses using Phase 1 for Design and Assessment and different loading discretization. Filled and empty markers indicate the attainment of shear failure (ShF) and maximum moment capacity (MoC) in ground floor columns cross-sections (see Figure 11), respectively.

505 The structural component assessment is done individually for each seaward column using *C+S* and

506 *C+D loading discretization*. Figure 16 presents the results of the pushover analyses with component

507 loading on a typical external column and on the corner seaward column (i.e. part of SMRF-1). The

508 worst load combination, presented in Figure 16a and b, occurs when the increased hydrodynamic

509 loading is applied to any of the external columns (see Figures 6c and d). The results for the *C+S loading*

510 *discretization* (Figure 16a) show that the external column with the increased component loading (e.g.

511 3011 column) experiences shear failure in both center and end sections for tsunami forces much smaller

512 than the LC2 design load. In this case, the LC2 tsunami force for half of the building is larger than

513 $F_{T,net,LC2}/2$ calculated for the *S loading discretization*, since it includes the increased drag force on the

514 component F_d and a share of the remainder $F_{T,net,LC2} - F_d$. The latter is assigned to all remaining columns

515 on the front of the structure, including those not present in the current model of half of the building (see

516 Figure 6c). Figure 156c plots the results for the component check on the ground floor corner column

517 (i.e. 10011) that fails in flexure and in shear, but later in the pushover analysis than the exterior column

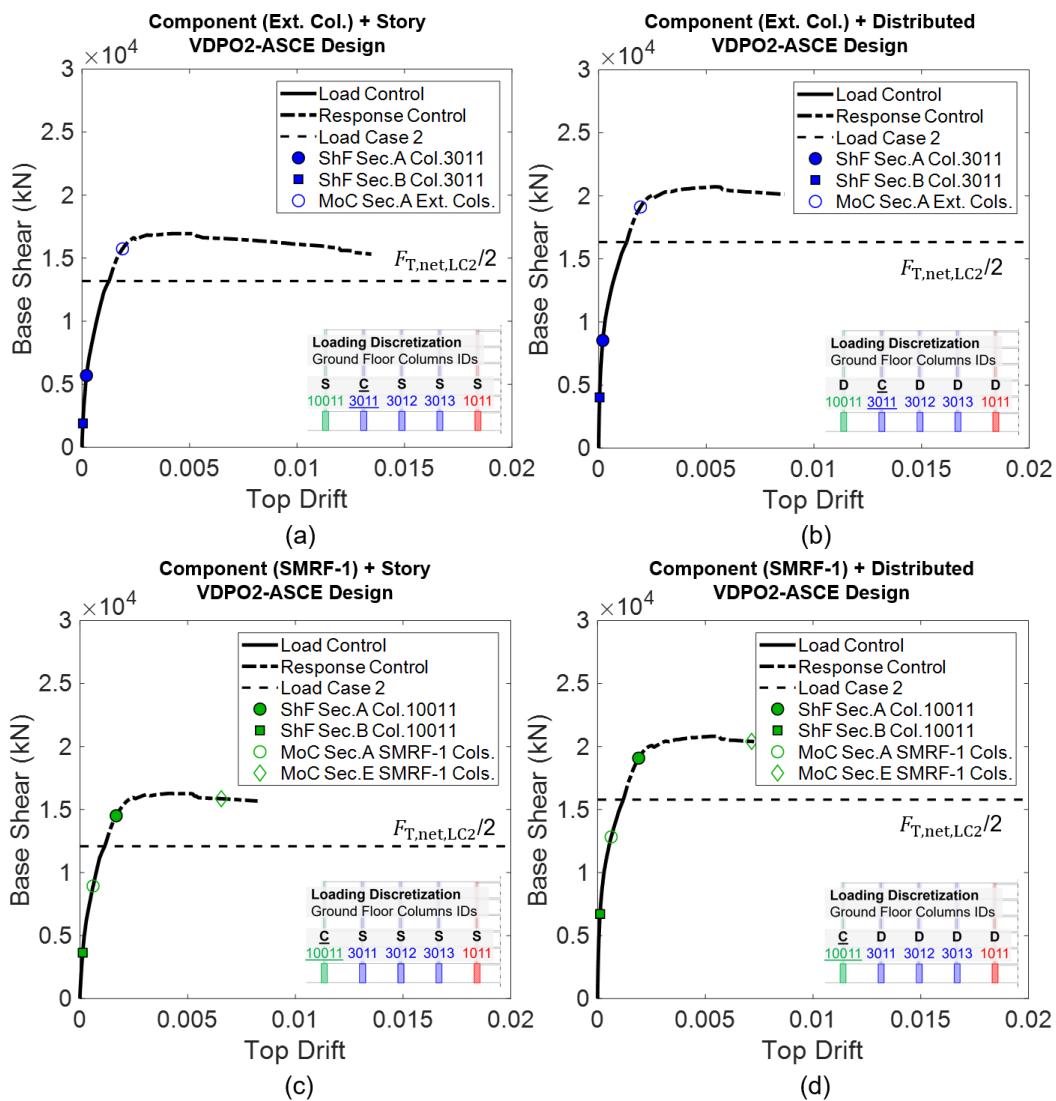518 as a result of the smaller hydrodynamic load tributary area for the corner column.

Figure 16: Base-shear-top drift curves for ASCE-VDPO2 analyses (Design): (a) *C+S loading discretization* for one line of external columns; (b) *C+D loading discretization* for one line of external columns; (c) *C+S loading discretization* for the corner column; and (d) *C+D loading discretization* for the line of corner column. Filled and empty markers indicate the attainment of shear failure (ShF) and maximum moment capacity (MoC) in ground floor column cross-sections (see Figure 11), respectively.

519   The pushover results for the *C+D loading discretization* are shown in Figures 16b and d for the

520   exterior column (3011) and the corner column (10011), respectively. The shear and flexural failure

521   points for the individual columns are equivalent to those observed in the *C+S loading discretization*

522   (Figures 16a and c) indicating that either *story (S)* or *distributed (D) loading discretization* can be used

523   to apply the remainder of the systemic load to the rest of the building while component distributed load

524   is applied to the columns being assessed.

525   If shear failure of the ground column is assumed as the structural failure criterion, the resulting

526   tsunami capacity of the building is approximately a third of the design tsunami load under the required

527   component loading combination. Therefore, the structure does not meet the collapse prevention

528   performance level required for taller risk category II buildings without additional strengthening of all

529   exterior and corner columns.

530   The use of a nonlinear static pushover analysis provides information on which components need to

531   be strengthened and by how much, in order to improve the tsunami performance of the structure. For

532   the case study building, this could be achieved by increasing the flexural and shear capacity of the

533   ground floor seaward and landward exterior columns. For instance, no shear failure would occur if shear

534   reinforcement is designed using #4 ties with 5-cm-spacing for all seaward column sections (Figure 12).

535   **CONCLUSIONS**

536   This study presents a methodology for using nonlinear static pushover analysis within the

537   framework of ASCE 7-16, called ASCE-VDPO2, and conducting the required systemic and component-

538   based design checks. An RC frame located in a high tsunami hazard area was considered as a case-

539   study. The ASCE-VDPO2 results were compared to the simplified ASCE 7-16 systemic tsunami

540   capacity acceptance criterion, which compares the overall tsunami force to the design seismic base

541   shear. The tsunami systemic capacity of the structure was seen to be sufficient to resist the ASCE 7-16

542   prescribed tsunami loads. However, the results highlighted that the relationship between the tsunami

543   and seismic strength of a building is not simple to predict. Hence, it is recommended in this paper that

544   non-linear structural tsunami analysis be used to conduct the systemic design check of ASCE 7-16

545   instead of the simplified check. The proposed procedure can also be used to assess the lateral force

546 resisting system for inundation depths and flow velocities larger than the ones for design basis event,

547 providing an estimate of the extra systemic capacity of the structure. When component loading was

548 considered, the seaward ground story columns were observed to fail in shear, precipitating structural

549 failure. Because ASCE 7-16 requires that the same hydrodynamic conditions be considered during both

550 incoming and outgoing tsunami flow, the seaward and landward ground story columns would need to

551 be strengthened in flexure and shear. This approach has the potential for providing a more economical

552 design as compared to the prescriptive ASCE 7-16 approach, which promotes an enhanced seismic

553 design of the structure to meet the systemic acceptance criteria of the standard. The methodology is also

554 expected to produce cost savings through its implementation. The authors are continuing this study to

555 investigate these savings.

556 It is noted that the tsunami response of the case-study structure is evaluated considering only the

557 effects of the tsunami-induced hydrodynamic loads. Other possible effects caused by tsunami, e.g.

558 buoyancy, debris impact, scour, as defined in the ASCE 7-16 Standard, are not considered in this study.

APPENDIX. BEST-FIT APPROXIMATION EQUATIONS FOR ASCE 7-16 TSUNAMI

559

560 **LOADS**

561 Table 1. List of best-fit approximation equations for the drag coefficient C_d in ASCE 7-16 Table 6.10-1.

Segment	B/h	Best-fit Approximation Equations
1	0–12	$C_d = 1.25$
2	12–16	$C_d = 0.0125 * B/h + 1.1$
3	16–36	$C_d = 0.01 * B/h + 1.14$
4	36–60	$C_d = 0.010417 * B/h + 1.125$
5	60–100	$C_d = 0.00125 * B/h + 1.675$
6	100–120	$C_d = 0.01 * B/h + 0.8$
7	>120	$C_d = 2$

562 Table 2. List of best-fit approximation equations for the normalized curves of tsunami inundation depths and flow velocity in
563 ASCE7-16 Figure 6.8-1.

Segment	t/T_{TSU}	Best-fit Approximation Equations ($x = t/T_{\mathrm{TSU}}$)
A	0–0.178	$h/h_{\max} = 3.745x$
B	0.178–0.5	$h/h_{\max} = 4.194x^3 - 7.457x^2 + 4.525x + 0.077$
C	0.5–0.822	$h/h_{\max} = -4.225x^3 - 5.19x^2 - 2.24x + 1.35$
D	0.822–1	$h/h_{\max} = -3.745x + 3.745$
E	0–0.033	$u/u_{\max} = 15.667x$
F	0.033–0.178	$u/u_{\max} = 75.24x^3 - 45.3x^2 + 9.98x + 0.235$
G	0.178–0.444	$u/u_{\max} = 0.527x^2 - 2.825x + 1.485$
H	0.444–0.556	$u/u_{\max} = -5.95x + 2.975$
J	0.556–0.822	$u/u_{\max} = -0.527x^2 - 1.77x + 0.813$

K	0.822–0.967	$u/u_{max} = 75.7x^3 - 181.7x^2 + 146.27x - 40.5$
L	0.967–1	$u/u_{max} = 15.667x - 15.667$

564 **DATA AVAILABILITY STATEMENT**

565 All data, models, and code that support the findings of this study are available from the

566 corresponding author upon reasonable request.

567 **ACKNOWLEDGMENTS**

572 **REFERENCES**

573 Aegerter (2021). "A Method for Conducting Push-over Tsunami Analysis in Accordance with

574 ASCE 7-16". MSc Thesis, University of Hawaii at Manoa.

575 Alam, M. S., Barbosa, A. R., Scott, M. H., Cox, D. T., and van de Lindt, J. W. (2017). "Development

576 of Physics-Based Tsunami Fragility Functions Considering Structural Member Failures." *ASCE J.*

577 *Struct. Eng.*, 144(3): 04017221.

578 ASCE (2017a), Minimum Design Loads and Associated Criteria for Buildings and Other

579 Structures. ASCE/SEI 7-16. Reston, VA, USA.

580 ASCE (2017b), Seismic Evaluation and Retrofit of Existing Buildings. ASCE/SEI 41-17, Reston,

581 VA, USA.

582 Attary, N., Unnikrishnan, V. U., van de Lindt, J.W., Cox, D. T., and Barbosa, A. R. (2017).

583 "Performance-Based Tsunami Engineering Methodology for Risk Assessment of Structures.", *Eng.*

584 *Struct.*, 141, 676–686.

585 Atwater, B. F., Stuivert, M., and Yamaguchi, D. K. (1991). "Radiocarbon Test of Earthquake

586 Magnitude at the Cascadia Subduction Zone." *Nature*, 353, pp. 156–158.

587   Baiguera, M., Rossetto, T., Robertson, I., and Petrone, C. (2019). "A nonlinear static procedure for

588   the tsunami design of a reinforced concrete building to the ASCE7 Standard." In: Rossetto, T, (ed.)

589   Proceedings of the SECED 2019 Conference. SECED: London, UK.

590   Chock, G. Y., Carden, L., Robertson, I. N., Wei, Y., Wilson, R., and Hooper, J. (2018). "Tsunami-

591   Resilient Building Design Considerations for Coastal Communities of Washington, Oregon, and

592   California." *ASCE J. Struct. Eng.*, 144(8):04018116.

593   Filippou, F. C., Popov, E. P., and Bertero, V. V. (1983). "Effects of Bond Deterioration on

594   Hysteretic Behavior of Reinforced Concrete Joints." Report EERC 83-19, Earthquake Engineering

595   Research Center, University of California, Berkeley.

596   Foster A. S. J., Rossetto T., Allsop W. (2017). "An experimentally validated approach for

597   evaluating tsunami inundation forces on rectangular buildings." *Coast. Eng. J.*, 128, pp. 44-57.

598   IBC (2018). International Building Code. Brea, CA: International Code Council.

599   Karsan, I.D., and Jirsa, J.O. (1969). "Behavior of concrete under compressive loading." *Journal of

600   Structural Division ASCE*, 95(ST12).

601   Kriebel, D. L., Lynett, P. J., Cox, D. T., Petroff, C. M., Riggs, H. R., Robertson I. N., and Chock

602   G. Y. K. (2017). "Energy Method for Approximating Overland Tsunami Flows." *Journal of Waterway,

603   Port, Coastal, and Ocean Engineering*, 143(5).

604   Macabuag, J., Lloyd, T., and Rossetto, T. (2014). "Sensitivity Analyses of a Framed Structure under

605   Several Tsunami Design-Guidance Loading Regimes." In Second ECES Conference. Istanbul.

606   McKamey, J., and Robertson, I. N. (2019). "Cost Implications for Including Tsunami Design in

607   Mid-Rise Buildings along the US Pacific Coast", Research Report. UHM/CEE/19-01.

608   McKenna, F., Scott, M. H., and Fenves, G. L. (2010) "Nonlinear finite-element analysis software

609   architecture using object composition." *Journal of Computing in Civil Engineering*, 24(1):95-107.

610   Petrone, C., Rossetto, T., and Goda, K. (2017). "Fragility Assessment of a RC Structure under

611   Tsunami Actions Via Nonlinear Static and Dynamic Analyses." *Eng Struct*, 136, pp. 36–53.

612   Petrone, C., Rossetto, T., Baiguera, M., De la Barra, C., and Ioannou, I. (2020). "Fragility Functions

613   for a Reinforced Concrete Structure Subjected to Earthquake and Tsunami in Sequence." *Eng. Struct.*,

614   205, 1102120.

615 Popovics, S. (1973). "A numerical approach to the complete stress strain curve for concrete. Cement

616 and Concrete Research." 3(5), 583-599.

617 Qi, Z. X., Eames, I., and Johnson, E. R. (2014). "Force Acting on a Square Cylinder Fixed in a

618 Free-Surface Channel Flow." *Journal of Fluid Mechanics,* 756, pp. 716–727.

619 Robertson, I. N. (2020). "Tsunami Loads and Effects: Guide to the Tsunami Design Provisions of

620 ASCE 7-16." ASCE, Reston, VA.

621 Rossetto, T., Petrone, C., Eames, I., De La Barra, C., Foster, A., and Macabuag, J. (2018).

622 "Advances in the Assessment of Buildings Subjected to Earthquakes and Tsunami." In: Pitilakis K.

623 (eds) Recent Advances in Earthquake Engineering in Europe. ECEE 2018. Thessaloniki, Greece.

624 Rossetto, T., De la Barra, C., Petrone, C., De la Llera, J. C., Vásquez, J., and Baiguera, M. (2019).

625 "Comparative assessment of nonlinear static and dynamic methods for analysing building response

626 under sequential earthquake and tsunami." *Earthquake Engng Struct Dyn.* 2019; 48: 867– 887.

627 Yokoyama, J., and Robertson, I. N. (2014). "Evaluation of Reinforced Concrete Buildings When

628 Subjected to Tsunami Loads." Research Report. UHM/CEE/14-01.